Anomalous Hall effect and magnetoresistance in the layered ferromagnet $Fe_{1/4}TaS_2$: The inelastic regime

J. G. Checkelsky,[1] Minhyea Lee,[1] E. Morosan,[2] R. J. Cava,[2] and N. P. Ong[1]
[1]*Department of Physics, Princeton University, Princeton, New Jersey 08544, USA*
[2]*Department of Chemistry, Princeton University, Princeton, New Jersey 08544, USA*
(Received 8 August 2007; published 22 January 2008)

The large magnetic anisotropy in the layered ferromagnet $Fe_{1/4}TaS_2$ leads to very sharp reversals of the magnetization **M** at the coercive field. We have exploited this feature to measure the anomalous Hall effect (AHE), focusing on the AHE conductivity σ_{xy}^A in the inelastic regime. At low temperature T (5–50 K), σ_{xy}^A is T independent, consistent with the Berry-phase/Karplus-Luttinger theory. Above 50 K, we extract an inelastic AHE conductivity σ_{xy}^{in} that scales as the square of $\Delta\rho$ (the T dependent part of the resistivity ρ). The term σ_{xy}^{in} clarifies the T dependence and sign reversal of the AHE coefficient $R_s(T)$. We discuss the possible ubiquity of σ_{xy}^{in} in ferromagnets and ideas for interpreting its scaling with $(\Delta\rho)^2$. Measurements of the magnetoresistance (MR) reveal a rich pattern of behavior vs T and field-tilt angle. We show that the two mechanisms, the anisotropic MR effect and field suppression of magnons, account for the intricate MR behavior, including the bow-tie features caused by the sharp reversals in **M**.

DOI: 10.1103/PhysRevB.77.014433 PACS number(s): 75.47.Np, 75.30.Gw, 75.50.Gg

I. INTRODUCTION

In a ferromagnet, the appearance of spontaneous magnetization breaks time-reversal symmetry (TRS) in the spin degrees of freedom. Spin-orbit coupling conveys the loss of TRS to the charge degrees. Hence, the appearance of spontaneous magnetization strongly influences the electrical currents. Although the investigation of this topic has had a very long history, interest in its many ramifications continues to surface, with each advance in understanding quantum effects in electron transport. The past seven years have seen strong resurgent interest—both theoretical[1–8] and experimental[9–17]—on the anomalous Hall effect (AHE), which is perhaps the most fascinating manifestation of TRS breaking in a ferromagnet. Recent research has clarified the fundamental relation between the Berry phase and the anomalous velocity which leads directly to the AHE when time-reversal invariance is broken. The notion of an anomalous velocity in a lattice has deep roots in the physics of solids, starting with the seminal 1954 theory of Karplus and Luttinger (KL).[18,19] The modern interest is also fueled by experiments to reverse magnetization by current in spin-based devices. These experiments explore anew issues pertaining to domain wall motion in applied currents and the reciprocal effects of domain motion on transport.[20]

We report transport experiments on the layered dichalcogenide ferromagnet $Fe_{1/4}TaS_2$, in which the spontaneous magnetization is strongly pinned perpendicular to the TaS_2 layers by a very large anisotropy field at temperatures T below the Curie point T_C (160 K).[21] In the hysteresis loops measured up to 100 K, reversal of **M** at the coercive field occurs as a very sharp jump ΔM, which induces a large jump $\Delta\sigma_{xy}$ in the Hall conductivity.[21] The ratio of the two quantities enables the anomalous Hall conductivity (AHC) to be accurately extracted. This allows us to address a major problem in the AHE in ferromagnets—the role of inelastic scattering at elevated T. Our analysis finds that the AHC is the sum of two terms of opposite signs. The first term, an intrinsic term independent of carrier lifetime, is identified with the Berry-phase/KL term. The second, increasingly dominant above 50 K, arises from inelastic scattering due to phonons and magnons. Closer to T_C, large fluctuations of the spins involve singular excitations which cannot be described by spin waves. We infer that these singular spin textures are responsible for much of the inelastic contribution to the AHE. The large magnitude of the inelastic AHE current implies that the scattering spin textures have chirality and may be related to topological singularities ("hedgehogs") which have been predicted to play a key role in disordering three-dimensional (3D) ferromagnets near T_C.[22] We isolate the inelastic term and show that it scales in as the square of the inelastic part of the resistivity. The complicated, nonmonotonic T dependence of the anomalous Hall coefficient $R_s(T)$ is then seen to be a simple consequence of competition between the Berry phase/KL term and the inelastic term. This competition seems to underlie the temperature profile of the AHE coefficient in many ferromagnets.

In ferromagnets, the magnetoresistance (MR) is dominated by two mechanisms.[14,23] One is the anisotropic magnetoresistance (AMR) effect in which the scattering rate for electrons with velocities $\mathbf{v}\|\mathbf{M}$ is higher than for $\mathbf{v}\perp\mathbf{M}$.[23–25] The second is the field suppression of magnons. The strong pinning of **M** to the c axis in $Fe_{1/4}TaS_2$ leads to a rich assortment of MR behavior apparent in field-tilt experiments. We show that the two mechanisms account very well for the full MR behavior, including the appearance of "bow-tie" features caused by the abrupt reversals in **M**. The analysis is considerably simplified because the two mechanisms dominate in opposite regimes of tilt angles and T. Both imply that scattering from spin excitations are dominant below T_C.

II. EXPERIMENTAL DETAILS

In the dichalcogenide TaS_2, the weak force between adjacent TaS_2 layers allows intercalation of most of the $3d$ transition-metal elements.[26] In the system Fe_xTaS_2, the

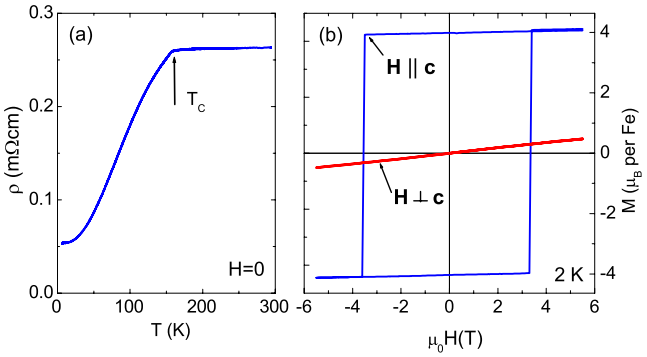

FIG. 1. (Color online) (a) The in-plane resistivity ρ vs T in $Fe_{1/4}TaS_2$ (H=0). At the Curie temperature T_C (arrow), $d\rho/dT$ has a discontinuity. (b) Curves of the magnetization M vs H at 2 K with $\mathbf{H}\|\mathbf{c}$ and $\mathbf{H}\perp\mathbf{c}$. The former shows a square shape with vertical jumps at the coercive fields H_c, while the latter is small and H linear.

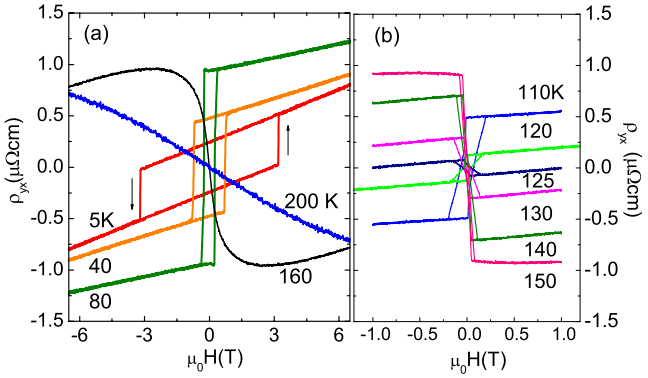

FIG. 2. (Color online) (a) The Hall resistivity ρ_{yx} vs H measured with $\mathbf{H}\|\mathbf{c}$ and $\mathbf{I}\perp\mathbf{c}$ at T=5, 40, 80, 160, and 200 K. Jumps in ρ_{yx} occur at H_c in response to the abrupt sign reversal of $\mathbf{M}$. Above T_C (T=160 and 200 K), ρ_{yx} is still dominated by the AHE term. (b) Expanded views of hysteresis loops of ρ_{yx} vs H for T near T_C. Note the reversal in circulation sense between 120 and 125 K.

ground state evolves from superconductivity to ferromagnetism with increasing x. A small Fe content (x=0.05) leads to a slight rise in the superconducting transition temperature T_c, but superconductivity is eventually destroyed.[27] At large x, the Fe ions order in a superlattice. The Curie transition to the ferromagnetic state occurs at T_C=40–160 K. In the specific interval $x=\frac{1}{4}\rightarrow\frac{1}{3}$, the easy axis of magnetization is perpendicular to the TaS_2 layers.[26] We focus on $Fe_{1/4}TaS_2$, in which the magnetic anisotropy is especially enhanced.

Single crystals of $Fe_{1/4}TaS_2$ were grown by iodine-vapor transport (see Ref. 21 for details on growth and sample characterization). The magnetization M was measured in a superconducting quantum interference device magnetometer. In the transport experiments, several crystals of typical size $\sim 1\times 0.2$ mm^2 and thickness $\leqslant 20$ μm were investigated using the standard four-probe ac lock-in technique. Electrical contacts, made by silver paint, had typical contact resistances smaller than 1 Ω. Rotation of the samples in a field was performed by a home-built rotation stage, which was in direct contact with the cold finger in the cryostat. The stage was suspended by sapphire V jewels strung by Kevlar lines to minimize heating during rotation. High-field measurements to 33 T were performed at the National High Magnetic Field Laboratory, Tallahassee.

III. RESISTIVITY AND MAGNETIZATION

We first discuss the T dependence of the in-plane resistivity ρ and magnetization M. Figure 1(a) shows that, above the Curie temperature T_C=160 K, ρ is nearly T independent. Below T_C, however, it drops by a factor of 4 from 160 to 4 K.

In the magnetic dichalcogenides $Cr_{1/3}NbS_2$ and $Fe_{1/4}NbSe_2$,[28] ρ is observed to vary smoothly across T_C. By contrast, the derivative $d\rho/dT$ in $Fe_{1/4}TaS_2$ displays a sharp discontinuity at T_C, which is likely a consequence of the unusually large magnetic anisotropy. Below T_C, $\mathbf{M}$ is strongly pinned to the (easy) axis $\mathbf{c}$ (normal to the layers). As shown in Fig. 1(b), the hysteretic M-H loop measured at 2 K has a rectangular shape with near-vertical jumps in M occurring at the coercive field H_c. In panel (b), the straight line with small slope represents the in-plane magnetization M_{ab} induced by $\mathbf{H}\perp\mathbf{c}$. The linear increase in M_{ab} implies that the in-plane susceptibility χ_{ab} is H independent up to 5.5 T. This H-independent χ_{ab} will prove useful in the analysis of the field-tilt MR. Further, assuming that the linearity in M_{ab} persists to intense H, we estimate that the anisotropy field H_A $\sim$60 T at 2 K. The jumps in M are observed to $T\sim$100 K.[21]

IV. ANOMALOUS HALL EFFECT

In the ferromagnetic state of $Fe_{1/4}TaS_2$, the Hall effect is a superposition of a term associated with the sharp jumps in M and an H-linear term associated with the Lorentz force. Figures 2(a) and 2(b) display the Hall resistivity (ρ_{yx}) in a field $\mathbf{H}\|\mathbf{c}$ with the current $\mathbf{I}$ in the ab plane. Clearly, the hysteresis loop of ρ_{yx} vs H at 5 K reflects the square magnetic hysteresis loop shown in Fig. 1(b). At $H=H_c$, ρ_{yx} suffers an abrupt sign reversal similar to that in M but is otherwise linear in H. By long practice, ρ_{yx} in a ferromagnet is empirically expressed as[29]

$$\rho_{yx} = R_H B + \mu_0 R_s M, \tag{1}$$

where μ_0 is the vacuum permeability and R_H and R_s are the ordinary and anomalous Hall coefficients, respectively. The first term is the ordinary Hall effect (OHE), while the second term R_sM is referred to as the anomalous Hall resistivity (ρ_{yx}^A).

In the elemental ferromagnets Fe and Ni, the AHE term is so much larger than the OHE term that one rarely worries about the latter.[29] However, in many magnetic systems of current interest (or in pure samples with very long electron mean free path ℓ), the OHE term is not negligible and often comparable in size. Then, the accurate separation of the two terms in Eq. (1) poses a difficult experimental problem. In Ref. 17, a method, based on scaling the MR curve against the M-H curve, was introduced for MnSi which has a very long ℓ at low T. Here, the abruptness of the jump in M provides

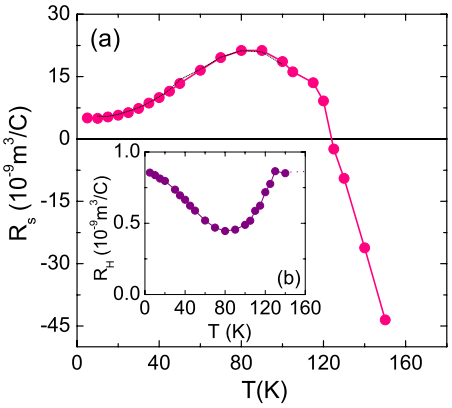

FIG. 3. (Color online) (a) The T dependence of the AHE coefficient R_s inferred from the jump in ρ_{yx} at H_c. (b) The OHE coefficient R_H vs T inferred from the H-linear portions of ρ_{yx}.

yet another way to execute this separation. As we tune H across H_c, inducing an abrupt jump and sign change in M, we engender a corresponding jump and sign change in ρ_{yx}. The ratio of the jump magnitudes ΔM and $\delta\rho_{yx}$ is a direct measurement of the AHE coefficient R_s, with minimal experimental uncertainty. The squareness of the M-H loop provides the most direct way to determine R_s in ferromagnets with a sizable OHE term. Away from the jump, the linear variation of ρ_{yx} with H is used to determine R_H. With this approach, we may reliably determine R_s and R_H at each T below T_C [Figs. 3(a) and 3(b)].

The OHE coefficient R_H is holelike and shows only a moderate T dependence with a broad minimum at ~80 K [Fig. 3(b)]. The Hall number density $n_H=1/eR_H$ varies from 0.8×10^{22} cm^{-3} at 5 K and to the peak value 1.4×10^{22} cm^{-3} at 80 K. The pronounced dip below T_C may reflect a strong change in the **k** dependence of the transport lifetime $\tau(\mathbf{k})$ around the FS.

How the anomalous Hall resistivity ρ_{yx}^A changes with T may be readily "read off" the loops by identifying the jump amplitude $\delta\rho_{yx}$ with $2\rho_{yx}^A$ [Figs. 2(a) and 2(b)]. At 5 K, R_s starts out positive—it circles the hysteresis loop in the same anticlockwise sense as M [arrows in Fig. 2(a)]. As T is raised, $\delta\rho_{yx}$ increases rapidly. However, the circulation changes sign near 125 K, above which ρ_{yx}^A becomes large and negative. The inferred anomalous Hall coefficient $R_s=\rho_{yx}^A/\mu_0 M$ is plotted in Fig. 3(a). Between 5 and 80 K, R_s increases by a factor of 6 to a broad maximum at 80 K. Then, it plunges to large negative values as $T\to T_C$, changing sign at ~125 K. The peaking of R_s and the sign reversal are common features of the R_s-T profile in many ferromagnets.[29,30] However, there has been scant progress in understanding its causes. We address this point in Sec. IV B.

Above T_C, ρ_{yx} is free of hysteresis. However, the negative sign of $d\rho_{yx}/dH$ for $T>T_c$ implies that ρ_{yx} is still dominated by the AHE term R_s. Despite the vanishing of the spontaneous M, field-induced alignment of the moments produces a large anomalous Hall response in the paramagnetic state (this is commonly observed in ferromagnets, e.g., in manganites[9]).

A. Intrinsic anomalous Hall effect conductivity at low T

In recent experimental approaches to the AHE problem, one prefers to focus on the Hall conductivities which have the very useful property of additivity (unlike ρ_{yx}). This view is emphasized in, e.g., Refs. 13 and 15–17. The total Hall conductivity σ_{xy} is the sum of the ordinary Lorentz-force Hall conductivity σ_{xy}^n and the AHC σ_{xy}^A,

$$\sigma_{xy}=\sigma_{xy}^n+\sigma_{xy}^A. \tag{2}$$

As the AHC scales with the magnetization M, we express it as[17]

$$\sigma_{xy}^A=S_H M, \tag{3}$$

where the scaling coefficient S_H has dimensions of V^{-1}. In MnSi, S_H is shown to be a constant below T_C.[17] Multiplying Eq. (2) across by ρ^2 and identifying σ_{xy}^n with $R_H\rho^2 H$, we have

$$\rho_{yx}=R_0 B+\mu_0 S_H\rho^2 M, \tag{4}$$

which is Eq. (1) with

$$R_s=S_H\rho^2. \tag{5}$$

The conductivity-additivity viewpoint emphasizes the constancy of the scaling parameter S_H, in contrast to R_s, which conflates the strong T and H dependences of the resistivity and σ_{xy}^A. This change of perspective involves more measurements, but it makes comparisons with quantities calculated in linear-response theory more direct (to theorists, R_s is a complicated empirical parameter that they usually ignore).

Adopting this approach, we display in Fig. 4(a) the hysteresis loops of the total Hall conductivity σ_{xy} inferred from the curves of $\rho_{yx}(H)$ and $\rho(H)$. As mentioned, the sharp jumps ΔM provide direct measurements of two Hall conductivities in Eq. (2). At each T, we identify the H-linear segments with σ_{xy}^n and the jump magnitudes with $2\sigma_{xy}^A$.

Figure 4(b) plots the T dependence of σ_{xy}^A from 5 to 125 K as solid circles. For comparison, we have also plotted the M vs T curve measured in a field of 0.1 T. There are two noteworthy features. Below 50 K, both the AHC and M are only very weakly T dependent, so they may be scaled together to give an estimate of $S_H=(1.93\pm0.07)\times10^4$ V^{-1} between M and $\Delta\sigma_{xy}$. This value is about 3.6 times smaller than in MnSi (where $S_H\sim7.04\times10^4$ V^{-1}).[17] The constancy of the AHC below 50 K is consistent with the KL prediction. The existence of the Berry-phase/KL AHC has now been established in several experiments.[11,12,15–17] For a simplified explanation of the Berry-phase/KL term, see Ref. 31.

B. Anomalous Hall effect in inelastic regime

The second important feature in Fig. 4(b) is the sharp downward deviation of σ_{xy}^A from M above 50 K. This deviation contrasts with the case in MnSi in which σ_{xy}^A is observed to track the curve of M right up to T_C (29 K).[17] The relatively sharp onset of the deviation here implies that a distinct contribution, negative in sign, appears at 50 K and grows rapidly in magnitude. This is rendered quite apparent if we plot the T dependence of the ratio σ_{xy}^A/M [to remove the T

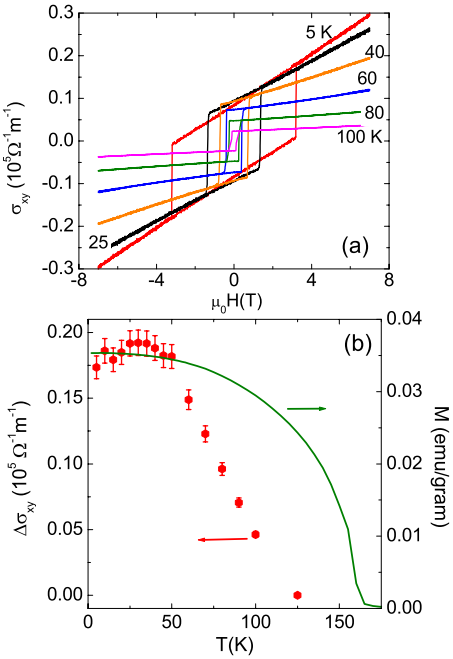

FIG. 4. (Color online) (a) Hysteresis loops of σ_{xy} [calculated from curves of $\rho_{yx}(H)$ and $\rho(H)$] at selected T. The H-linear segments are the classical Lorentz component, while the jumps are the AHC σ_{xy}^A. (b) The T dependence of the jump magnitude $\Delta\sigma_{xy}=2\sigma_{xy}^A$ (solid circles). For comparison, we also plot M measured at 0.1 T (solid curve). Note that the jump magnitude is T independent below 50 K within our resolution. Above 50 K, it falls steeply to negative values.

dependence of $M(T)$] [Fig. 5(a)]. The constancy of the ratio from 5 to 50 K (discussed in the previous section) gives way to a steep decrease above 50 K, consistent with the appearance of a negative contribution to the AHC (shaded region).

As the new term's magnitude increases monotonically with T, we identify it with a Hall conductivity σ_{xy}^{in} caused by scattering from inelastic excitations, notably magnons and spin defects or textures in the uniform magnetization. To include this term, the AHC in Eq. (3) (divided by M) becomes

$$\frac{\sigma_{xy}^A}{M}=S_H+\frac{\sigma_{xy}^{in}}{M}, \tag{6}$$

where the two terms on the right have opposite signs. Subtracting off the constant S_H, we display the T dependence of the new term $-\sigma_{xy}^{in}/M$ in Fig. 5(b). This brings out the monotonic increase in $-\sigma_{xy}^{in}/M$ which extends from 50 K to $\sim T_C$. In magnitude, $|\sigma_{xy}^{in}|/M$ is equal to S_H near 125 K but continues to grow to $\sim 1.5\ S_H$ at T_C. To underscore its origin in inelastic excitations, we have compared it with the inelastic part of the resistivity $\Delta\rho(T)=\rho(T)-\rho(0)$ (the MR is negligible in the geometry with $\mathbf{H}\|\mathbf{c}$). Remarkably, $-\sigma_{xy}^{in}/M$ matches very well the curve of $(\Delta\rho)^2$ [solid curve in panel (b)]. Scaling to $(\Delta\rho)^3$ is much less satisfactory.

We remark that the isolation of the term σ_{xy}^{in} (Fig. 5) rests on the sole assumption that the Berry-phase/KL term S_H is T independent up to T_C, which has an experimental support from Refs. 15–17. Independent of this assumption, the existence of a large inelastic term in the AHC is immediately apparent from inspection of the raw data of ρ_{yx} (Fig. 2). The jumps $\delta\rho_{yx}=2\sigma_{xy}^A/\rho^2$ are seen to remain at a large value even though M decreases rapidly as $T\to T_C^-$ (see curves at 130, 140, and 150 K). This requires an AHC term that is large and negative. We discuss this further in Sec. VI.

As mentioned in Sec. I, a difficult aspect of the AHE problem is the issue of inelastic excitations. To complicate matters, the T dependence of the AHE, by long practice, is usually reported in terms of $R_s(T)$, which mixes the T dependences of ρ and σ_{xy}^A (Sec. IV A). In a broad class of ferromagnets, the profile of $R_s(T)$ follows a common pattern.[9,29] Typically, R_s starts out small at low T and increases rapidly as a power law of T to attain a broad peak at $\sim 0.8\ T_C$. As T crosses T_C, R_s decreases gradually into the paramagnetic

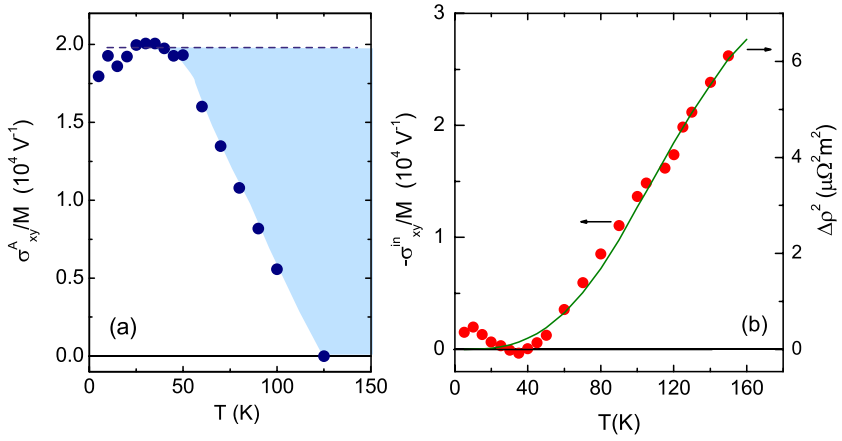

FIG. 5. (Color online) (a) The T dependence of the anomalous Hall conductivity divided by magnetization σ_{xy}^A/M and (b) comparison of the inelastic component σ_{xy}^{in}/M with $(\Delta\rho)^2$. In panel (a), σ_{xy}^A/M is expected to be the constant S_H (dashed line). However, above 50 K, a negative contribution σ_{xy}^{in}/M appears and increases rapidly in magnitude (shaded region). σ_{xy}^{in} is the Hall conductivity produced by inelastic excitations. Panel (b) shows that the T dependence of σ_{xy}^{in}/M (solid circles) matches the square of $\Delta\rho$ (inelastic part of resistivity, solid curve).

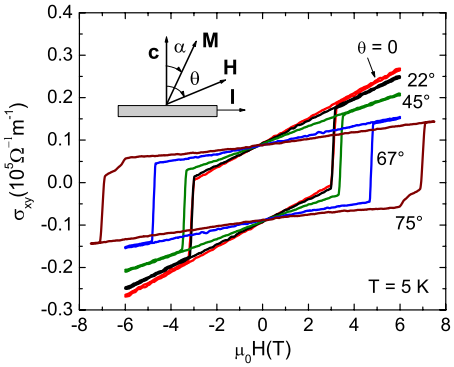

FIG. 6. (Color online) Hysteresis loops of σ_{xy} at $T=5$ K at selected field-tilt angles θ. Although the H-linear segments (OHE component) changes as $\cos\theta$ (scaling as $\mathbf{H}\cdot\mathbf{c}$), the jump magnitude (AHE component) is nominally independent of θ. The inset defines the tilt angles α and θ relative to $\mathbf{c}$ of $\mathbf{M}$ and $\mathbf{H}$, respectively.

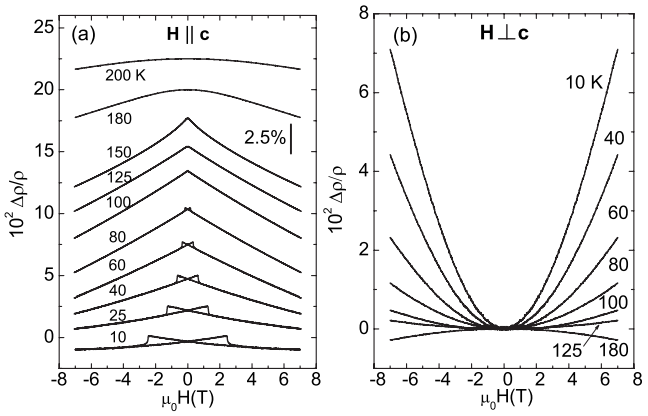

FIG. 7. Magnetoresistance curves at selected temperatures in the field geometry (a) $\mathbf{H}\|\mathbf{c}$ and (b) $\mathbf{H}\perp\mathbf{c}$. In panel (a), the MR is negative and nominally H linear indicating the dominance of the magnon-suppression mechanism. The curves are displaced vertically by 2.5% for clarity. The bow-tie features correspond to jumps $\delta\rho$ at H_c (Sec. V C). In panel (b), the MR is positive with H^2 variation, reflecting the AMR effect. The current $\mathbf{I}\perp\mathbf{c}$ in both panels.

state. Often, but not always, R_s changes sign just below T_C, as it does here [Fig. 3(a)].

The isolation of $\sigma_{xy}^{in}(T)$, which is opposite in sign to the KL term and strictly monotonic in T, clarifies significantly the T profile of $R_s(T)$. By Eqs. (5) and (6), we have

$$R_s(T) = \rho(T)^2\left[S_H + \frac{\sigma_{xy}^{in}}{M}\right]. \tag{7}$$

At low T, σ_{xy}^{in} is negligible. With the assumption that S_H is a constant, R_s initially increases as ρ^2. As σ_{xy}^{in}/M grows to dominate S_H in the interval 80–120 K, the quantity within $[\cdots]$ steadily decreases, changing sign near 125 K. The steep increase in the prefactor ρ^2 causes R_s to go through a broad peak before plunging to large negative values. Hence, the simple dependence $\sigma_{xy}^{in}\sim(\Delta\rho)^2$ directly accounts for the profile of $R_s(T)$.

The angular dependence of the AHC is shown in Fig. 6 (at 5 K where inelastic excitations are negligible). The size of the jump $\Delta\sigma(\theta)$ is nominally independent of θ, consistent with the results in Fig. 4(b). Since the AHC is determined only by $\mathbf{M}$, it follows that the direction and magnitude of $\mathbf{M}$ are nominally independent of the field-tilt angle θ. By contrast, the H-linear segments which represent the OHE scale as $\cos\theta$, i.e., the component of H normal to $\mathbf{I}$. An interesting feature is seen in the curve at $\theta=75°$. The rounding of the corner of the hysteretic loop is attributed to the reversible rotation of M just below the coercive field.[32]

V. MAGNETORESISTANCE

The MR displays a rich assortment of behaviors depending on the field geometry. The MR curves measured with the current $\mathbf{I}$ in the ab plane are displayed in Figs. 7(a) and 7(b) in the configurations $\mathbf{H}\|\mathbf{c}$ and $\mathbf{H}\perp\mathbf{c}$, respectively. In the latter, we align $\mathbf{H}\|\mathbf{I}$ to minimize carrier deflections by the Lorentz force. In panel (a), the MR is always negative and nominally H linear. The relative decrease is largest just below T_C but becomes much weaker as $T\to 10$ K. Below 100 K, the jumps in M at the coercive fields H_c produce jumps in ρ that become more prominent at low T (the jumps are discussed in Sec. V C). By sharp contrast, the MR in panel (b) shows quite the opposite trend as T decreases below T_C. Below 100 K, the MR is positive and quadratic in H. Its magnitude increases dramatically as $T\to 10$ K.

We have investigated the angular dependence of the MR to learn more about the MR. Figure 8(a) shows the MR curves measured at 5 K for a series of tilt angles $\theta=0°,\ldots,90°$ (θ is the angle between $\mathbf{H}$ and $\mathbf{c}$; see the inset in Fig. 6). With increasing tilt, the MR curve, initially negative, becomes strongly positive with an H^2 dependence. However, the same sequence of measurements at 80 K [Fig. 8(b)] shows a different trend. The slope of the nominally linear curves at $\theta=0$ weakens substantially as $\theta\to 90°$. The overall patterns in Figs. 7(a) and 7(b) and Figs. 8(a) and 8(b) suggest the existence of two competing MR contributions, one that is positive with an H^2 variation and the other that is H linear and negative.

A. Anisotropic magnetoresistance

At low T, a dominant contribution to the MR is the AMR effect, in which the resistivities $\rho_\|$ and $\rho_\perp$ (measured with $\mathbf{I}\|\mathbf{M}$ and $\mathbf{I}\perp\mathbf{M}$, respectively) differ measurably. In most experiments, the difference $\rho_\Delta\equiv(\rho_\|-\rho_\perp)$ is found to be positive. The AMR has been explained[23–25] by an anisotropy in the scattering of carriers in the s band to a d state and back to the s band without spin flip,

$$|4s,\mathbf{k}\downarrow\rangle\to|3d\downarrow\rangle\to|4s,\mathbf{k}'\downarrow\rangle.$$

The spin-orbit term $\lambda\mathbf{L}\cdot\mathbf{S}$ leads to mixing of the d spin states $|d\uparrow\rangle$ and $|d\downarrow\rangle$, while the direction of $\mathbf{M}$ imparts a vector direction that, in effect, enhances the scattering amplitude for electrons moving with velocity $\mathbf{v}\|\mathbf{M}$ over those with $\mathbf{v}\perp\mathbf{M}$. This anisotropic selectivity, intrinsically tied to s-d transi-

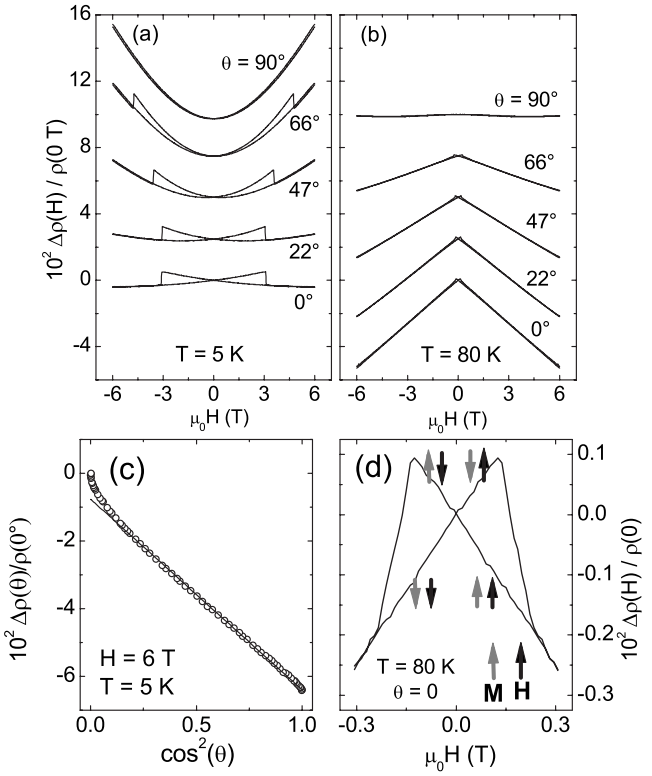

FIG. 8. The MR curves measured at selected field-tilt angles $\theta = 0°, \ldots, 90°$ (with $\mathbf{I} \perp \mathbf{c}$) at (a) 5 K and (b) 80 K. Curves are displaced by 2.5% for clarity. As θ increases in panel (a), the AMR mechanism is increasingly dominant (positive MR and H^2). However, in panel (b), the magnon-suppression mechanism, dominant at $\theta=0$, progressively weakens as $\theta \uparrow 90°$. In panel (c), the MR measured at 5 K in $H=6$ T is plotted against $\cos^2\theta$. The solid line is a fit to Eq. (9). Panel (d) is an expanded view of the bow-tie hysteresis loop of ρ caused by the jumps in $\mathbf{M}$, measured with $\mathbf{H} \| \mathbf{c}$ at $T=80$ K. Black (gray) arrows represent directions of $\mathbf{H}$ ($\mathbf{M}$) at selected segments of loop.

tions that do not flip spin, tends to be suppressed when inelastic scattering processes that flip the spin are important. Hence, the AMR mechanism weakens rapidly in the presence of magnon scattering at elevated T. A study of the AMR and the planar Hall effect in Fe and Fe_3Si films has been recently reported.[33]

In the field-tilt experiments, we alter the respective fractions of carriers with $\mathbf{v} \| \mathbf{M}$ and $\mathbf{v} \perp \mathbf{M}$ by changing the tilt angle α of $\mathbf{M}$ relative to $\mathbf{c}$ (we keep $\mathbf{I} \perp \mathbf{c}$; see inset in Fig. 6).[14] To leading order in α, the AMR is expressed as

$$\rho(\alpha) = \rho_\perp + \rho_\Delta \sin^2(\alpha). \tag{8}$$

It is more convenient to express the MR in terms of the angle θ between $\mathbf{H}$ and $\mathbf{c}$. Using χ_{ab} to eliminate α, we have

$$\rho(\theta) = \rho_\perp + \rho_\Delta \left[\frac{\chi_{ab} H}{M_s}\right]^2 - \rho_\Delta \left[\frac{\chi_{ab} H}{M_s}\right]^2 \cos^2(\theta), \tag{9}$$

where M_s is the saturated magnetization. The fit of Eq. (9) to the MR data taken at 5 K with $H=6$ T is quite good [Fig. 8(c)]. The fit yields a large $\rho_\Delta = +260\ \mu\Omega$ cm that is more than five times $\rho(H=0\ \text{T})$ (the positive sign of ρ_Δ is similar

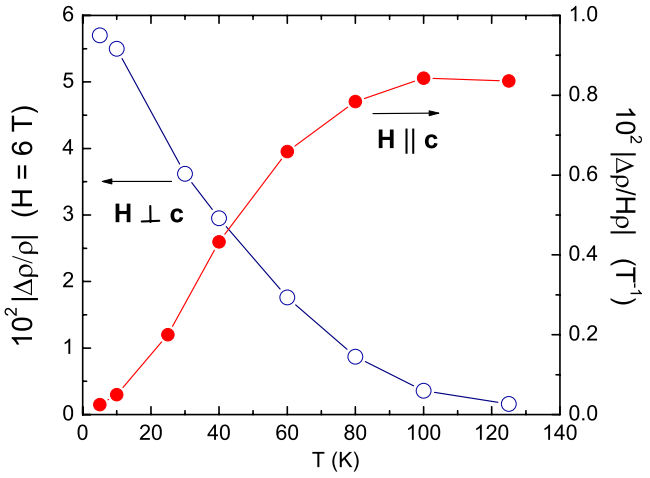

FIG. 9. (Color online) The T dependence of the MR signals measured with $\mathbf{H} \perp \mathbf{c}$ (open circles) and $\mathbf{H} \| \mathbf{c}$ (closed). For $\mathbf{H} \perp \mathbf{c}$, the MR signal is the fractional change $\Delta\rho(T,H)/\rho(T,0)$ measured at 6 T. For $\mathbf{H} \| c$, we have plotted the initial slope of the fractional change $\Delta\rho(T,H)/\rho(T,0)H$ $(H \to 0)$.

to that in most ferromagnets). The AMR effect leads to positive MR with an H^2 dependence up to at least 14 T. Consequently, the AMR is dominant in the MR curves with $\mathbf{H}$ at a sizable tilt angle θ [Figs. 7(b) and 8(a)].

The T dependence of the MR data is displayed in Fig. 9. In the geometry with $\mathbf{H} \perp \mathbf{c}$ (open circles), the MR signal, reported as the fractional increase $\Delta\rho(T,H)/\rho(T,0)$ with H fixed at 6 T, decreases sharply from 5.8% at 5 K to 0.1% at 120 K. This is as expected if the AMR mechanism dominates the MR in this geometry.

By contrast, with $\mathbf{H} \| \mathbf{c}$, $\mathbf{M}$ remains pinned to $\| \mathbf{c}$, so the AMR is very weak. The MR is then dominated by the magnon-suppression mechanism discussed in the next section (Sec. V B). The (negative) MR signal increases with T, consistent with magnon suppression (closed circles in Fig. 9).

We have also made limited MR measurements in high fields, up to 31 T (Fig. 10). The high-field MR with $\mathbf{H} \perp \mathbf{c}$ taken at 1.5 K (bold curve) shows significant deviation from

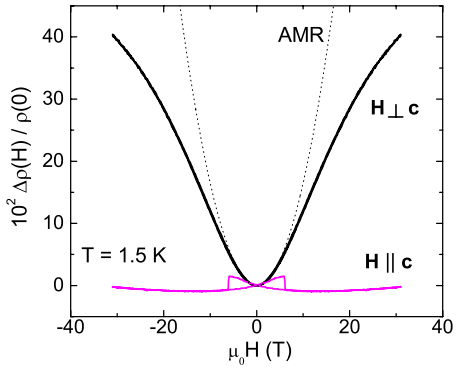

FIG. 10. (Color online) Magnetoresistance measured to 31 T with $\mathbf{H} \perp \mathbf{c}$ (bold curve) and $\mathbf{H} \| \mathbf{c}$ (faint curve with bow-tie feature). The dashed curve is the weak-field AMR expression [Eq. (9)].

the H^2 trend of Eq. (9) (dashed curve) above 10 T, confirming that the in-plane susceptibility χ_{ab} gets smaller as the tilt angle α of $\mathbf{M}$ gets large, as expected. From the 40% change in ρ at 31 T, we calculate that $\alpha \sim 15°$. In the geometry $\mathbf{H} \| \mathbf{c}$ (faint curve), the MR is negative and shows a prominent bow tie but is quite small overall. Above 15 T, we detect an H^2 upturn associated with orbit bending by the Lorentz force. This curve shows the field scale needed to detect the classical orbital contribution to the MR in perpendicular field.

B. Field suppression of magnons

The second important contribution to the MR in ferromagnets is the field suppression of the magnon population. In applied field, the Zeeman energy stiffens the restoring force against thermally induced fluctuations of the moments away from equilibrium, thereby raising the energies of magnon branches. The consequent decrease in magnon population reduces the scattering of the carriers. The effect depends only on the component of $\mathbf{H} \| \mathbf{M}$. Hence, for $\mathbf{H} \| \mathbf{M}$, one observes a negative MR with H-linear variation (reflecting the H-linear increase in Zeeman energy).[14,34] The negative MR curves observed in the geometry $\mathbf{H} \| \mathbf{c}$ are consistent with this magnon-suppression mechanism. In Fig. 7(a), the fractional decrease $\Delta\rho/\rho$, at, say, 6 T rises rapidly from 5 to 150 K. We quantify the negative, H-linear MR by the initial slope of the fractional change in ρ, viz., $\Delta\rho(T,H)/\rho(T,0)H$. Its T dependence, revealing a sharp increase in the interval 5–100 K, is consistent with the increased dominance of magnon scattering at elevated T (solid circles in Fig. 9). As mentioned, this trend is opposite to that of the AMR effect (open circles).

The reversal in dominance of the two mechanisms is also evident in the field-tilt experiment (Fig. 8). At low T [panel (a)], increasing θ converts the weak negative MR (weak magnon suppression) to a large positive H^2 MR (dominant AMR). However, at high T [80 K, panel (b)], the opposite is observed. The magnon suppression is dominant at $\theta=0$ but nearly unresolved at 90°.

C. Resistance jumps at coercive field

The abrupt reversal of $\mathbf{M}$ at $-H_c$ causes a jump in the resistivity $\delta\rho$ to produce the bow-tie feature in Fig. 8(d). Both the AMR and magnon-suppression mechanisms contribute to the jump $\delta\rho$, with the latter dominant at elevated T. In the metastable state, with $-\mathbf{M} \| \mathbf{H}$, the Zeeman energy serves to *soften* the restoring force against deviations $\delta\mathbf{M}$, so that the magnon population is enhanced by field. Thus, as H increases in the negative direction, ρ increases until reversal of $\mathbf{M}$ occurs at $H=-H_c$. Then, the magnons adjust to the equilibrium population causing ρ to jump downward, as seen in the curves with $\mathbf{H} \| \mathbf{c}$ at high T.

At very low T, however, the exponential decrease in the magnon population renders the magnon-suppression mechanism ineffectual. Yet, the jump magnitude $\delta\rho$ is seen to increase to large values at 0.3 K (curve at 1.5 K in Fig. 10). In this limit, we reason that $\delta\rho$ mostly comes from the AMR effect. In the metastable state, the demagnetization field exerts a strong force on the pinned magnetization, particularly near the edge of the crystal. This causes the magnetization vector $\mathbf{M}(\mathbf{r})$ to splay, producing a weak gradient in tilt angle $\alpha(\mathbf{r})$ [$\alpha(\mathbf{r})$ varies from 0 in the center to a value α_0 at the edge]. Although the average $\langle\alpha\rangle=0$ over the sample volume, the mean of the square $\langle\alpha^2\rangle$ is finite. By Eq. (8), the gradient leads to an AMR. From the measured $\delta\rho/\rho \sim 1.5\%$ and the magnitude of ρ_Δ obtained above, we estimate that $\alpha_0 \sim 0.1°$. Thus, a very slight gradient in $\mathbf{M}(\mathbf{r})$ is sufficient to account for the jump magnitude at 0.3 K.

VI. DISCUSSION

In $Fe_{1/4}TaS_2$, the jump in $\mathbf{M}$ provides a way to accurately determine the anomalous Hall conductivity. From the analysis of the T dependence of the AHC, we find that it is T independent from 5 to 50 K, despite an increasing ρ. This behavior is consistent with the Berry-phase/KL theory which predicts that the AHC is dissipationless (independent of the carrier transport lifetime τ). Any residual T dependence comes from $M(T)$ via Eq. (3). In a few ferromagnets, $La_{1-x}Sr_xCoO_3$ (Ref. 16) and MnSi,[17] this is found to be the case over an extended interval of T up to the T_C. However, in the majority of ferromagnets, the AHE coefficient $R_s(T)$ displays a strong T dependence (and often a sign reversal), which indicates a more complicated picture at elevated T. Despite the accumulating evidence in support of the validity of the Berry-phase/KL theory at low T, the role of inelastic excitations is poorly understood.

Here, we find that a negative, inelastic term σ_{xy}^{in} becomes resolved above 50 K and increases rapidly in magnitude as $T \to T_C^-$. We show that the nonmonotonic complicated T profile of R_s is accounted for as a sum of this term and a positive KL term σ_{xy}^{KL} [Eq. (7)]. As mentioned, the isolation of σ_{xy}^{in} rests on the assumption that the KL term is strictly given by $S_H M(T)$ with S_H a constant.

As shown in Fig. 5(b), the inelastic AHC scales as $(\Delta\rho)^2$. Expressed in terms of τ, we have $\sigma_{xy}^{in} \sim 1/\tau^2$. This rules out, as the origin of the inelastic term, skew scattering[29,35] which scales as $\sigma_{xy}^{skew} \sim \tau$.

We sketch our ideas on interpreting the inelastic AHC term σ_{xy}^{in}. Its strong T dependence suggests that it is more insightful to view this term as a transverse current arising from scattering off spin excitations, whose density $n_s(T)$ rises rapidly with T. At low T, these are magnons. However, as $T \to T_C$, the large fluctuations in the order parameter render the spin-wave picture invalid, and singular or large-amplitude fluctuations involving spin textures dominate. Numerical simulations[22] have shown that spontaneous pair production of topological singularities (dubbed hedgehogs) plays a crucial role in the ferromagnetic-to-paramagnetic transition in the 3D Heisenberg model. Our results suggest that such chiral excitations contribute strongly to the AHC.

We assume that $n_s(T)$ includes both spin waves and these singular excitations. From the MR results in Sec. V, the T dependence of ρ is dominated by scattering from spin excitations, i.e., $\Delta\rho \sim n_s(T)$. Our finding then implies $\sigma_{xy}^{in} \sim n_s(T)^2$. If each spin excitation generates a contribution to the Hall current, we should have measured a linear depen-

dence on n_s. The higher power n_s^2 implies that the Hall current selectively responds to certain correlations between nearby spin excitations. In the Hall studies on manganite[9] and pyrochlore,[10] it is argued that a Berry-phase Hall current is produced by correlations between local moments. Hopping between three spins that subtend a finite solid angle Ω (finite chirality $\mathbf{S}_1 \cdot \mathbf{S}_2 \times \mathbf{S}_3$) forces the electron to acquire a geometric Berry phase $\chi_B \sim \Omega$, which translates into a large Hall current (this is distinct from the KL AHE). Likewise, we may expect that scattering of Bloch-state electrons from fluctuating spins leads to a large Hall current that selectively responds to regions with large average chirality $\langle \mathbf{S}_1 \cdot \mathbf{S}_2 \times \mathbf{S}_3 \rangle$. This mechanism is analyzed in the calculations in Refs. 1 and 4. The results in Fig. 5(b) suggest that the AHE in the inelastic regime in $Fe_{1/4}TaS_2$ involves the Berry phase arising from scattering from spin fluctuations with finite chirality.

The rich behavior in the magnetoresistance is also consistent with the presence of two spin-related mechanisms, AMR and magnon suppression. The classical Lorentz-force mechanism is insignificant until H exceeds $\sim$15 T (at low T). Although the arguments are largely qualitative, the broad range of measurements provides a fairly objective test that we find highly persuasive. In the geometry $\mathbf{H} \perp \mathbf{c}$, the AMR is dominant with magnon suppression unobserved, so the MR is positive, increasing as H^2. The suppression of AMR with increasing inelastic excitations accounts for the steep fall of the MR at high T in this geometry. However, with $\mathbf{H} \| \mathbf{c}$, the magnon-suppression mechanism is dominant, while AMR is inoperative. Accordingly, the MR is negative and nominally H linear. The increase in the MR signal with T is consistent with the magnon-suppression mechanism. Finally, the jump magnitude of the resistance at H_c is explained by the combination of these two mechanisms.

ACKNOWLEDGMENTS

We have benefitted from discussions with N. Nagaosa, S. Maekawa, and S. Onoda. Research at Princeton University was supported by the U.S. National Science Foundation (NSF) under Grant No. DMR 0213706. The high-field measurements were performed at the National High Magnetic Field Laboratory, Tallahassee, a national facility supported by NSF and the State of Florida.

[1] J. Ye, Y. B. Kim, A. J. Millis, B. I. Shraiman, P. Majumdar, and Z. Tešanović, Phys. Rev. Lett. **83**, 3737 (1999).
[2] G. Sundaram and Q. Niu, Phys. Rev. B **59**, 14915 (1999).
[3] M. Onoda and N. Nagaosa, J. Phys. Soc. Jpn. **71**, 19 (2002).
[4] G. Tartara and H. Kawamura, J. Phys. Soc. Jpn. **71**, 2613 (2002).
[5] T. Jungwirth, Q. Niu, and A. H. MacDonald, Phys. Rev. Lett. **88**, 207208 (2002).
[6] Y. Yao, L. Kleinman, A. H. MacDonald, J. Sinova, T. Jungwirth, D.-S. Wang, E. Wang, and Q. Niu, Phys. Rev. Lett. **92**, 037204 (2004).
[7] F. D. M. Haldane, Phys. Rev. Lett. **93**, 206602 (2004).
[8] S. Onoda, N. Sugimoto, and N. Nagaosa, Phys. Rev. Lett. **97**, 126602 (2006).
[9] P. Matl, N. P. Ong, Y. F. Yan, Y. Q. Li, D. Studebaker, T. Baum, and G. Doubinina, Phys. Rev. B **57**, 10248 (1998).
[10] Y. Taguchi, Y. Oohara, H. Yoshizawa, N. Nagaosa, and Y. Tokura, Science **291**, 2573 (2001).
[11] W.-L. Lee, S. Watauchi, V. L. Miller, R. J. Cava, and N. P. Ong, Science **303**, 1647 (2004).
[12] R. Mathieu, A. Asamitsu, H. Yamada, K. S. Takahashi, M. Kawasaki, Z. Fang, N. Nagaosa, and Y. Tokura, Phys. Rev. Lett. **93**, 016602 (2004).
[13] N. Manyala, Y. Sidis, J. F. DiTusa, G. Aeppli, D. P. Young, and Z. Fisk, Nat. Mater. **3**, 255 (2004).
[14] W. Gil, D. Görlitz, M. Horisberger, and J. Kötzler, Phys. Rev. B **72**, 134401 (2005).
[15] C. Zeng, Y. Yao, Q. Niu, and H. H. Weitering, Phys. Rev. Lett. **96**, 037204 (2006).
[16] Y. Onose and Y. Tokura, Phys. Rev. B **73**, 174421 (2006).
[17] M. Lee, Y. Onose, Y. Tokura, and N. P. Ong, Phys. Rev. B **75**, 172403 (2007).
[18] R. Karplus and J. M. Luttinger, Phys. Rev. **95**, 1154 (1954).
[19] E. I. Blount, in *Solid State Physics*, edited by H. Ehrenreich, F. Seitz, and D. Turnbull (Academic, New York), Vol. 13, p. 305.
[20] For a review, see S. Maekawa, *Concepts in Spin Electronics* (Oxford University Press, Oxford, 2006).
[21] E. Morosan, H. W. Zandbergen, L. Li, M. Lee, J. G. Checkelsky, M. Heinrich, T. Siegrist, N. P. Ong, and R. J. Cava, Phys. Rev. B **75**, 104401 (2007).
[22] M.-H. Lau and C. Dasgupta, Phys. Rev. B **39**, 7212 (1989); M. Kamal and G. Murthy, Phys. Rev. Lett. **71**, 1911 (1993).
[23] T. R. McGuire and R. I. Potter, IEEE Trans. Magn. **11**, 4 (1975).
[24] J. Smit, Physica (Amsterdam) **21**, 877 (1951).
[25] I. A. Campbell, A. Fert, and O. Jaoul, J. Phys. C **3**, S95 (1970).
[26] S. S. P. Parkin and R. H. Friend, Philos. Mag. B **41**, 65 (1980); **41**, 95 (1980).
[27] Z. Dai, Q. Xue, Y. Gong, C. G. Slough, and R. V. Coleman, Phys. Rev. B **48**, 14543 (1993).
[28] M. Lee, T. Klimzuck, R. J. Cava, and N. P. Ong (unpublished).
[29] C. Hurd, *The Hall Effect in Metals and Alloys* (Plenum, New York, 1972), Chap. 5, pp. 153–182.
[30] Y. Kats, I. Genish, L. Klein, J. W. Reiner, and M. R. Beasley, Phys. Rev. B **70**, 180407(R) (2004).
[31] N. P. Ong and W.-L. Lee, *Foundations of Quantum Mechanics in the Light of New Technology*, edited by S. Ishioka and K. Fujikawa (World Scientific, Singapore, 2006), p. 121; arXiv:cond-mat/0508236.
[32] H. Kronmüller, K.-D. Durst, and G. Martinek, J. Magn. Magn. Mater. **69**, 149 (1987).
[33] K.-J. Friedland, M. Bowen, J. Herfort, H. P. Schönherr, and K. H. Ploog, J. Phys.: Condens. Matter **18**, 2641 (2006).
[34] B. Raquet, M. Viret, J. M. Broto, E. Sondergard, O. Cespedes, and R. Mamy, J. Appl. Phys. **91**, 8129 (2002); B. Raquet, M. Viret, E. Sondergard, O. Cespedes, and R. Mamy, Phys. Rev. B **66**, 024433 (2002).
[35] J. Smit, Physica (Amsterdam) **21**, 877 (1955).